Biochem. J. (2011) **433**, 163–174 (Printed in Great Britain) doi:10.1042/BJ20101353

Mesohaem substitution reveals how haem electronic properties can influence the kinetic and catalytic parameters of neuronal NO synthase

Jesús TEJERO*[1,2], Ashis BISWAS*[1,3], Mohammad Mahfuzul HAQUE*, Zhi-Qiang WANG*†, Craig HEMANN‡, Cornelius L. VARNADO§, Zachary NOVINCE*, Russ HILLE‖, Douglas C. GOODWIN§ and Dennis J. STUEHR*[4]

*Department of Pathobiology, Lerner Research Institute, Cleveland Clinic Foundation, Cleveland, OH 44195, U.S.A., †Department of Chemistry, Kent State University Tuscarawas, New Philadelphia, OH 44663, U.S.A., ‡The Davis Heart and Lung Research Institute, Ohio State University, Columbus, OH 43210, U.S.A., §Department of Chemistry and Biochemistry, Auburn University, Auburn, AL 36849, U.S.A., and ‖Department of Biochemistry, University of California Riverside, Riverside, CA 92521, U.S.A.

NOSs (NO synthases, EC 1.14.13.39) are haem-thiolate enzymes that catalyse a two-step oxidation of L-arginine to generate NO. The structural and electronic features that regulate their NO synthesis activity are incompletely understood. To investigate how haem electronics govern the catalytic properties of NOS, we utilized a bacterial haem transporter protein to overexpress a mesohaem-containing nNOS (neuronal NOS) and characterized the enzyme using a variety of techniques. Mesohaem-nNOS catalysed NO synthesis and retained a coupled NADPH consumption much like the wild-type enzyme. However, mesohaem-nNOS had a decreased rate of Fe(III) haem reduction and had increased rates for haem−dioxy transformation, Fe(III) haem−NO dissociation and Fe(II) haem−NO reaction with O_2. These changes are largely related to the 48 mV decrease in haem midpoint potential that we measured for the bound mesohaem cofactor. Mesohaem nNOS displayed a significantly lower V_{max} and K_mO_2 value for its NO synthesis activity compared with wild-type nNOS. Computer simulation showed that these altered catalytic behaviours of mesohaem-nNOS are consistent with the changes in the kinetic parameters. Taken together, the results of the present study reveal that several key kinetic parameters are sensitive to changes in haem electronics in nNOS, and show how these changes combine to alter its catalytic behaviour.

Key words: electron transfer, flavoprotein, haemprotein, mesohaem, nitric oxide, nitric oxide synthase (NOS).

INTRODUCTION

NO (nitric oxide) is a signalling molecule with a wide range of functions in biology [1]. In animals NO is synthesized from L-Arg (L-arginine) by enzymes known as NOSs (NO synthases, EC 1.14.13.39). Three isoforms of NOS are found in mammals: eNOS (endothelial NOS), nNOS (neuronal NOS) and iNOS (inducible NOS). All three are homodimers, with each subunit consisting of an N-terminal oxygenase domain that contains protoporphyrin IX (haem) and binding sites for BH_4 (tetrahydrobiopterin) and L-Arg, and a C-terminal reductase domain that includes binding sites for NADPH and the cofactors FAD and FMN. A CaM (calmodulin)-binding sequence is also located between the two domains [2−4]. The NO synthesis reaction proceeds in two steps that each require NADPH and O_2, and generates NOHA (N^{ω}-hydroxy-L-Arg) as an enzyme-bound intermediate (Figure 1A). During catalysis, electrons from NADPH transfer through the bound FAD and FMN to the haem in NOS, and haem reduction is CaM-dependent [5]. The reduced [Fe(II)] haem binds O_2 and then receives an electron from the bound BH_4, generating a BH_4 radical in the process. The electron transfer from BH_4 is critical because it enables the formation of haem−oxy species that ultimately react with L-Arg and NOHA [6−8].

To understand how the electronic properties of the haem can influence its function in proteins, one useful approach has been to replace the native haem with other metallo-porphyrins or with haem structural analogues [9−20]. Haem substitution in NOS enzymes has been accomplished using both insect cell and *Escherichia coli* expression systems [9,10]; however, the resulting NOS proteins were only characterized regarding their spectral properties and steady-state NO synthesis activities. Because the activity of NOS is determined by several kinetic parameters that describe both its inherent NO synthesis and NO dioxygenase activities [6,21,22] (Figure 1B), it is essential to study how manipulations such as haem substitution affect the individual kinetic parameters [6] in order to understand how haem substitution influences NOS catalysis.

Until now, the influence of haem electronics on NOS kinetic parameters (Figure 1B) has only been probed indirectly through site-directed mutagenesis of a proximal-side tryptophan residue that interacts with the haem−thiolate bond [23−27]. As an alternative more direct approach, we co-expressed a haem-transporter protein [28] in *E. coli* in order to incorporate Fe−mesoporphyrin IX (mesohaem) into full-length nNOS and the nNOSoxy (nNOS oxygenase domain). Mesohaem contains ethyl groups in place of the 2- and 4-vinyl groups on the protoporphyrin ring, and has been useful as a tool to alter haem electronics in a variety of other haemproteins [9−20]. In the present study we analysed how the mesohaem substitution has an impact on the thermodynamic, kinetic and catalytic properties

Abbreviations used: BH_4, tetrahydrobiopterin; CaM, calmodulin; DTT, dithiothreitol; EPPS, 4-(2-hydroxyethyl)-1-piperazinepropanesulfonic acid; L-Arg, L-arginine; NOHA, N^{ω}-hydroxy-L-Arg; NOS, NO synthase; nNOS, neuronal NOS; nNOSoxy, nNOS oxygenase domain; TFA, trifluoroacetic acid.

[1] These authors contributed equally to this work.

[2] Present address: Vascular Medicine Institute of the University of Pittsburgh, University of Pittsburgh School of Medicine, BST3 Room 10051, 3501 5th Avenue, Pittsburgh, PA 15260, U.S.A.

[3] Present address: School of Basic Sciences (Chemistry), Indian Institute of Technology Bhubaneswar. Bhubaneswar, Orissa 751013, India

[4] To whom correspondence should be addressed (email stuehrd@ccf.org).

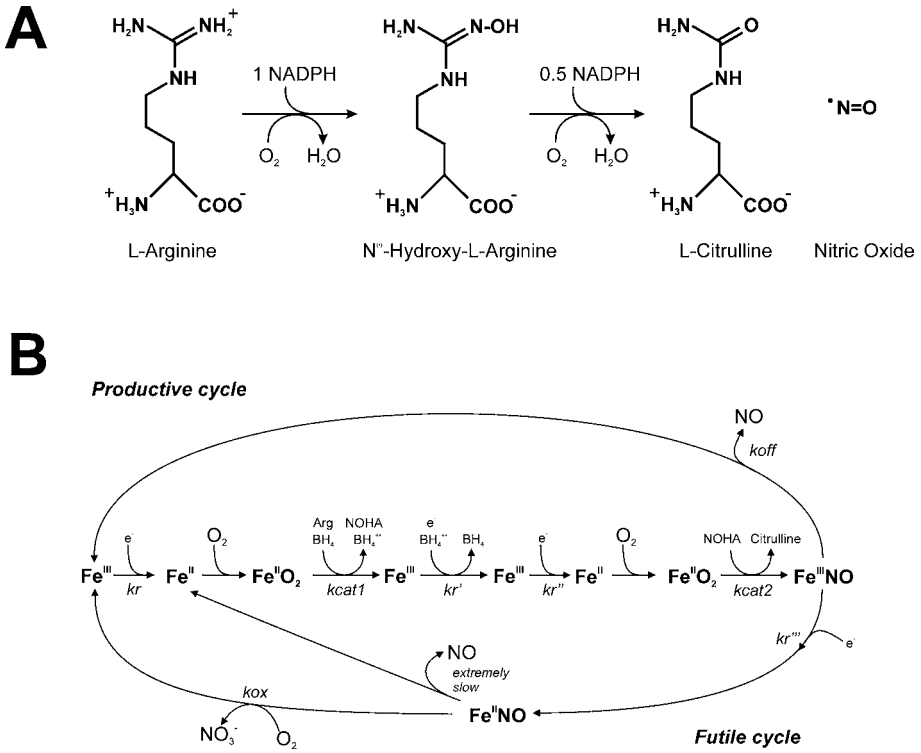

Figure 1 Biosynthesis of NO by NOS enzymes

(**A**) NO synthesis from L-Arg. NOS catalyses the hydroxylation of arginine to form the NOHA intermediate and then the oxidation of NOHA to citrulline releasing NO. (**B**) Global kinetic model for NOS. The reduction of Fe(III) enzyme (*kr*) is the rate-limiting step for the NO biosynthetic reactions (central linear portion). This electron transfer is needed to reduce the Fe(III) haem before each catalytic step (*kr*, *kr''*) and also to reduce the BH_4 radical between cycles (*kr'*). *kcat1* and *kcat2* are the conversion rates of the Fe(II)—O_2 species to products in the consecutive L-Arg and NOHA reactions respectively. The Fe(III) haem—NO product complex [Fe(III)—NO] can either release NO (*koff*) or be reduced by the flavoprotein domain (*kr'''*) to a Fe(II) haem—NO complex [Fe(II)—NO], which reacts with O_2 (*kox*) in an NO dioxygenase reaction to regenerate the nitrate and Fe(III) enzyme.

of nNOS. Moreover, we used our measured kinetic values in computer simulations of a global kinetic model for NOS catalysis (Figure 1B) [6,21,22] to determine whether the changes we measure can explain the catalytic behaviours of mesohaem-substituted nNOS. Taken together, the results of the present study improve our understanding of how haem electronics help to control catalysis by NOS enzymes.

EXPERIMENTAL

Reagents

BH_4 was purchased from Schircks Laboratories. CO and NO gases were obtained from Praxair. EPPS [4-(2-hydroxyethyl)-1-piperazinepropanesulfonic acid] was purchased from Fisher Scientific. DTT (dithiothreitol) was purchased from RPI Corporation. Fe-protoporphyrin IX and Fe-mesoporphyrin IX were purchased from Frontier Scientific. All other reagents were purchased from Sigma.

Protein expression and purification

Full-length nNOS and nNOSoxy (amino acids 1—720) were overexpressed as described previously to obtain the protoporphyrin IX-containing proteins [29,30]. To produce the proteins containing mesoporphyrin IX, a different strategy was used [28]. First, *E. coli* BL21(DE3) were transformed with plasmids containing the pHPEX2 plasmid encoding the haem transporter gene *chuA* [28] (tetracycline-resistant) and either the full-length nNOS or nNOSoxy protein (ampicillin-resistant). Then, 500 ml of M9 minimal medium supplemented with 10 ml/l of BME (basal medium Eagle) vitamin solution (Sigma), 0.4 % Bacto™ casamino acids (BD Biosciences), 125 μg/ml ampicillin and 15 μg/ml tetracycline was inoculated with 10 ml of an overnight culture of *E. coli* BL21(DE3) harbouring the nNOS and pHPEX2 plasmids and cultured at 37 °C, 250 rev./min, until the attenuance (*D*) was 0.8—1.0. Induction of nNOS was initiated by addition of 1 mM IPTG (isopropyl β-D-thiogalactopyranoside) and 0.75 μM (for full-length nNOS) or 1.5 μM (for nNOSoxy) Fe(III)- mesoporphyrin IX chloride. The cultures were then grown at room temperature (25 °C), and cells were harvested after 24 h. Subsequent purification steps were carried out as described previously [29,30].

Quantification of haem content using an HPLC assay

Haem was extracted by mixing 200 μl of full-length nNOS or nNOSoxy protein ($\sim$1 mg) with 1 ml of acetone containing 3 % HCl for 10 min at room temperature. Then, these solutions were centrifuged at 10000 ***g*** for 20 min to get rid of any precipitated materials. The amount of total haem bound to protein was quantified using an HPLC method. Samples were first diluted with water (1:1) and then 50 μl of diluted sample was injected on to a Alltech ODS-Partisil, 5 μm particle size, 4.6 mm $\times$ 250 mm reverse-phase C_{18} HPLC column and eluted at a flow rate of 1.0 ml/min with linear gradients of buffers A [0.1 % TFA (trifluoroacetic acid) in water] and B (0.1 % TFA in 80 % acetonitrile). The solvent gradient was as follows: 0—10 min,

55–65 % B; 10–14 min, 65–90 % B; then the buffer B amount was decreased to a final value of 55 % within 14–18 min. Absorption at 280 and 400 nm was monitored. Under these conditions, Fe-protoporphyrin IX and Fe-mesoporphyrin IX were eluted at 3.5 and 7.7 min respectively. Standard curves were produced for the different porphyrins and used to calculate the haem content. Each sample was analysed in triplicate.

UV–visible spectra

Absorbance spectra were determined using Cary-50 Bio, Cary 100 Bio or Shimadzu UV2401PC spectrophotometers with quartz cuvettes. In some cases anaerobic conditions were required [haem–Fe(II), Fe(II)–NO and Fe(III)–NO complexes] and anaerobic cells with an attached quartz cuvette were used.

Redox potentiometry

Redox titrations were carried out in a glovebox (Belle Technology) under an atmosphere of nitrogen as described previously [31]. Protein samples at approx. 10 μM were made anaerobic inside the glovebox by gel filtration in a Sephadex G25-column (PD10, GE Healthcare) equilibrated with anaerobic buffer [0.1 M potassium phosphate (pH 7.0) and 125 mM NaCl]. After elution, the samples were diluted to a 7 ml final volume and BH_4 (25 μM) and L-Arg (2.5 mM) was added. Measurements were carried out at 15 ± 1 °C. Redox mediators (Sigma) 1–5 μM anthraquinone-2-sulfonate (E_m -225 mV), phenosafranine (E_m -252 mV) and Benzyl Viologen (E_m -358 mV) were used. A correction factor of $+209$ mV at 15 °C was used [31]. The fraction of protein oxidized for each spectrum was calculated from the maximum difference between oxidized and reduced spectra (approx. 430 nm and 390 nm). The fraction oxidized was plotted against the potential [compared with the SHE (standard hydrogen electrode)] and analysed by non-linear regression via the Nernst equation [32] using the Origin 7.5 software (OriginLab). Reported values for the redox potential measurements are means $\pm$ S.D. of three or more determinations. Actual errors may be larger as other factors such as electrode accuracy or equilibration errors are not factored into the calculations.

NO synthesis, NADPH oxidation and electron flux measurement

Steady-state activities of wild-type nNOS and mesohaem-nNOS proteins were determined at 25 °C using the spectrophotometric oxyhaemoglobin assay as reported previously [33]. Cuvettes contained 0.1–0.2 μM NOS, 40 mM EPPS (pH 7.6), 150 mM NaCl, 0.3 mM DTT, 4 μM FAD, 4 μM FMN, 10 μM BH_4, 5 mM L-Arg or 250 μM NOHA, 1 mg/ml BSA, 1.0 mM Ca^{2+}, 0.25 mM EDTA, 1.0 μM CaM, 100 units/ml catalase, 25 units/ml superoxide dismutase and 5 μM oxyhaemoglobin. The reaction was initiated with 250 μM NADPH in a total reaction volume of 500 μl and was run for 2 min. In the assays without CaM, neither CaM nor $CaCl_2$ was added. For the electron flux measurement through the NOS haem during steady-state catalysis, we measured the rate of NADPH oxidation by each CaM-bound enzyme in the absence of L-Arg substrate or in the presence of 2.0 mM agmatine [25,34].

Haem reduction

The electron transfer from the reductase domain to the haem was studied at 10 °C, as described previously [33] using a Hi-Tech SF-61 stopped-flow instrument with diode array detector (TgK Scientific) equipped for anaerobic work. A protein solution containing 10 μM nNOS, 100 mM EPPS (pH 7.6), 100 mM NaCl, 10 μM BH_4, 2 mM L-Arg, 0.5 mM DTT, 50 μM CaM, 5 mM $CaCl_2$ and 1mM EDTA, at least half CO-saturated, was mixed with an anaerobic CO-saturated solution containing 100 mM EPPS (pH 7.6), 100 mM NaCl and 100 μM NADPH. Haem reduction was followed by the formation of the Fe(II)–CO complex with a maximum of approx. 444 nm (wild-type) or 430 nm (mesohaem). The time course of the absorbance changes was fitted to a bi-exponential equation, where the first phase (absorbance decrease) was assigned to the flavin reduction, and the subsequent absorbance increase was assigned to haem reduction. The signal-to-noise ratio was improved by averaging data from six or more individual mixing experiments.

Single-turnover reactions

A single-turnover reaction of nNOSoxy proteins with oxygen in the presence of L-Arg or NOHA was carried out as descibed previously [35,36]. Anaerobic solutions of nNOSoxy (10–15 μM) containing 50 μM BH_4, either 1 mM L-Arg or 0.5 mM NOHA, 1 mM DTT, 150 mM NaCl and 10 % glycerol in 40 mM EPPS buffer (pH 7.6) were made anaerobic and then the protein was titrated with dithionite. The reduced protein was mixed with air-saturated buffer in the stopped-flow apparatus at 10 °C. The data were fitted to an Fe(II)→Fe(II)–O_2→Fe(III) model for L-Arg reaction or to an Fe(II)→Fe(II)–O_2→Fe(III)–NO→Fe(III) for the NOHA reaction. Spectral data were fitted to these models using the Specfit/32 global analysis software software, Version 3.0 (Spectrum Software Associates). Data from six or more reactions were averaged to obtain the final traces.

Stoichiometry of L-Arg hydroxylation

A solution containing 1 mM wild-type nNOSoxy or mesohaem-bound nNOSoxy, 3 mM L-Arg, 1.0 mM BH_4, 0.5 mM DTT, 10 % glycerol and 150 mM NaCl in 40 mM EPPS buffer (pH 7.6) was made anaerobic and titrated with sodium dithionite to produce the Fe(II) enzyme. Different amounts of these stock solutions were mixed with air-saturated buffer containing 3 mM L-Arg, 10 % glycerol and 150 mM NaCl in 40 mM EPPS (pH 7.6) at room temperature. These reaction mixtures were incubated for 10 min to ensure completeness and were then quenched by adding 5 μl of 1.0 M HCl to the reaction mixtures (total volume 100 μl) and the samples were stored at -70 °C. NOHA formed in these samples were estimated by HPLC as described previously [37]. Product yields are indicated as means $\pm$ S.E.M. for three experiments.

Oxidation of Fe(II) haem–NO complexes

The reaction of Fe(II)–NO complexes with oxygen were studied as described previously [21]. Protein solutions containing 10 μM Fe(III) NOSoxy were prepared in 40 mM EPPS buffer (pH 7.6), 10 % glycerol, 150 mM NaCl, 20 μM BH_4, 2.5 mM L-Arg and 0.5 mM EDTA. Protein samples were made anaerobic by several cycles of nitrogen/vacuum. Then, Fe(III) haem was titrated with sodium dithionite to produce the Fe(II) enzyme. The reduced enzyme was then titrated with an NO-saturated buffer solution until the red-shift of the Soret band was complete. The resulting protein Fe(II)–NO complexes were rapidly mixed with air-saturated buffer (oxygen concentration 357 μM at 10 °C) with the same composition as the protein buffer. Reactions were carried out at 10 °C in a Hi-Tech SF-61 stopped-flow instrument equipped with a diode array detector.

BH_4 radical formation

An anaerobic solution containing reduced mesohaem-nNOSoxy (150 μM), 200 μM L-Arg, 0.5 mM BH_4, 0.1 mM DTT, 10 % glycerol and 150 mM NaCl in 40 mM EPPS buffer (pH 7.6) was mixed with oxygen-saturated EPPS buffer at 10 °C. Protein samples after different mixing times were obtained by rapid-freeze techniques using a modified Hi-Tech RQF-63 rapid quench instrument (TgK Scientific) as described previously [35]. EPR spectra were recorded in a Bruker ER300 instrument equipped with an ER 035 NMR gauss meter and a Hewlett-Packard 5352B microwave power controller. Spectra were obtained at 150 K using a microwave power of 2 mW, a frequency of 9.5 GHz, a modulation amplitude of 10 G and a modulation frequency of 100 kHz. In order to improve the signal-to-noise ratio, ten scans per sample were accumulated.

Measurement of apparent K_mO_2

Apparent K_m and V_{max} values were calculated by fitting the initial rates of NO synthesis measured at various oxygen concentrations to a hyperbolic equation using the Origin 7.5 software (OriginLab) [34,38]. Reactions were carried out in septum-sealed cuvettes that contained 0.2 μM NOS (wild-type nNOS or mesohaem-nNOS), 40 mM EPPS (pH 7.6), 150 mM NaCl, 0.3 mM DTT, 4 μM FAD, 4 μM FMN, 10 μM BH_4, 5 mM L-Arg, 1 mg/ml BSA, 1.0 mM $CaCl_2$, 0.25 mM EDTA, 1.0 μM CaM, 100 units/ml catalase, 25 units/ml superoxide dismutase and 5 μM oxyhaemoglobin diluted in various ratios of N_2-, air- or O_2-saturated buffer solutions. The reaction was initiated with 250 μM NADPH in a total reaction volume of 800 μl and was carried out for 2 min at 25 °C. The initial O_2 concentration in each reaction was calculated based on the solution mixing ratio and the O_2 concentration of air- or O_2-saturated buffer at 25 °C (approx. 0.26 and 1.26 mM respectively).

nNOS distribution during steady-state NO synthesis

The distribution of the different NOS species on steady-state conditions was calculated by the global model (Figure 1B) as implemented in Mathcad 7.0 [21,22]. Small modifications were introduced to account for the haem and BH_4 radical reduction steps [39,40]. The simulations assume constant values for $[O_2] = 180$ μM and [NADPH] = 40 μM. The values for haem reduction (k_r), NO dissociation (k_{off}) and Fe(II) haem−NO oxidation (k_{ox}) were $k_{ox} = 0.08$ s^{-1}, $k_r = 6.6$ s^{-1} and $k_{off} = 5.1$ s^{-1} for wild-type nNOS and $k_{ox} = 0.192$ s^{-1}, $k_r = 1.09$ s^{-1} and $k_{off} = 8.2$ s^{-1} for mesohaem-nNOS. The other values were the same for both simulations: $k_2 = k_5 = 135$ s^{-1}, $k_3 = k_6 = 26$ s^{-1} and $k_9 = 0.001$ s^{-1}. Reaction numbering as in [39].

Kinetics of enzyme Fe(II) haem−NO complex formation

Enzyme spectral transitions during the initial phase of NO synthesis were studied at 10 °C in the Hi-Tech SF-61 stopped-flow instrument with a diode array detector as described previously [24,41,42]. To initiate NO synthesis, an air-saturated solution containing 40 mM EPPS (pH 7.6), 10 % glycerol, 150 mM NaCl, ~8 μM wild-type nNOS or mesohaem-nNOS enzyme, 20 μM BH_4, 0.4 mM DTT, 3 mM L-Arg, 0.5 mM EDTA, 2 mM Ca^{2+} and 40 μM CaM was rapidly mixed with an air-saturated buffered solution containing 50 μM NADPH. Absorbance scans were recorded and the absorbance at 436 nm or at 424 nm (for wild-type nNOS and mesohaem-nNOS respectively) was utilized to follow Fe(II) haem−NO formation, and absorbance at 340 nm was utilized to follow NADPH oxidation [24,41,42]. Signal-to-noise ratios were improved by averaging at least ten individual mixing experiments. Each experiment was performed with two enzyme preparations.

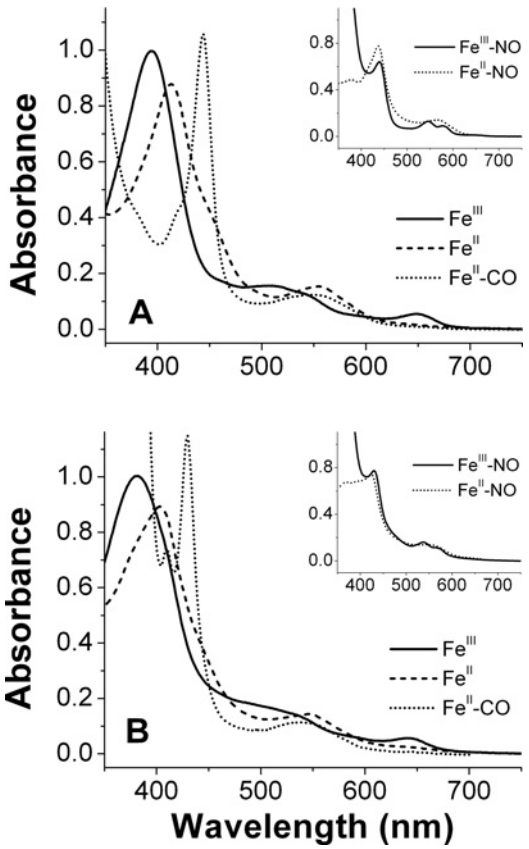

Figure 2 Spectral properties of the wild-type and mesohaem-containing nNOSoxy proteins

The spectra for the Fe(II), Fe(III), Fe(II)−CO, Fe(II)−NO and Fe(III)−NO complexes are shown. (**A**) Wild-type nNOSoxy domain; (**B**) mesohaem-containing nNOSoxy domain.

RESULTS AND DISCUSSION

Generation of mesohaem-nNOS proteins

The minimal medium cultures of *E. coli* BL21(DE3) cells containing the nNOS and pHPEX2 expression plasmids produced nNOS proteins with yields of 1−5 mg/l for full-length nNOS and 5−10 mg/l for nNOSoxy, which were then purified to >90 % as judged by SDS/PAGE (results not shown). Both nNOS proteins were ~85−90 % dimeric in the presence of BH_4 and L-Arg as judged by gel filtration (results not shown) [43], consistent with earlier reports on mesohaem-nNOS [9]. HPLC analyses of haem content gave ratios of mesohaem-to-protohaem of 95:5 for nNOSoxy and 92:8 for full-length nNOS (results not shown). These ratios were as good or better than those reported in other haem substitution studies with NOS [9,10] and indicate that the proteins would be suitable for detailed studies.

UV−visible spectra of mesohaem-nNOS

We recorded spectra of the Fe(III), Fe(II) and the Fe(II)−CO, Fe(II)−NO and Fe(III)−NO complexes of the mesohaem-substituted nNOSoxy and full-length nNOS proteins (Figure 2 and Table 1). Compared with wild-type nNOS, we observed a consistent blue-shift of between 8 and 15 nm in the peak Soret

Table 1 Absorbance maxima for wild-type and mesohaem-nNOS proteins

Peak values are in nm.

Haem species	Wild-type nNOSoxy	Wild-type full-length nNOS	Mesohaem-nNOSoxy	Full-length mesohaem-nNOS
Fe(III)	395, 649	394, 649	381, 641	379, 641
Fe(II)	413, 554	411, 553	403, 547	400, 548
Fe(II)−CO	444,549	444, 551	430, 539	430, 540
Fe(III)−NO	440, 546, 577	438, 545, 578	430, 538, 563	430, 539, 566
Fe(II)−NO	437, 565	437, 567	424, 548	424, 555

Table 2 NO synthesis and NADPH oxidation rates of wild-type nNOS and mesohaem-nNOS proteins with different substrates or analogues and in the presence or absence of bound CaM

Values were determined at 25 °C. Rates are in s^{-1}. Values shown are means ± S.E.M.

Activity	Substrate or analogue	Wild-type nNOS	Mesohaem-nNOS
NO synthesis (+CaM)	L-Arg	47 ± 3	34 ± 2
	NOHA	91 ± 8	62 ± 1
NADPH oxidation (+CaM)	L-Arg	97 ± 10	65 ± 4
	NOHA	103 ± 9.5	70 ± 4
	L-Agmatine	352 ± 28	92 ± 7
	None	368 ± 32	97 ± 8
NADPH oxidation (−CaM)	L-Arg	7.0 ± 0.6	9 ± 1
	NOHA	11.5 ± 1	11 ± 1

absorbance of the mesohaem-substituted proteins, accompanied by lesser but significant blue-shifts in their visible bands (Figure 2 and Table 1). The position of the Fe(II)−CO Soret peak (430 nm) in our mesohaem-nNOSoxy and full-length nNOS matches the previously reported values for mesohaem-nNOS [9], and our preparations have a minor Soret absorbance at 410 nm that indicates the presence of a 'P420' species, which was present in greater amounts in the earlier studies [9,10]. An absence of a second peak or shoulder at 445 nm for the Fe(II)−CO complex confirms that a negligible amount of protoporphyrin IX is present in our proteins. In general, the shifts to shorter wavelength that we observed in the mesohaem-nNOS spectra are similar to shifts observed for other mesohaem-substituted proteins [12−16], and arise because the mesoporphyrin ring has less π-electron conjugation and is more electron-rich compared with protoporphyrin.

Steady-state catalytic activities

The steady-state NO synthesis activities of mesohaem-nNOS with either L-Arg or NOHA as substrate, and the corresponding NADPH oxidation rates, are compared with wild-type values in Table 2. The NO synthesis activities of mesohaem-nNOS were decreased by 25 % and 32 % respectively with these substrates, relative to wild-type nNOS. The NADPH oxidation rates we measured during NO synthesis (+CaM, Table 2) show that the mesohaem substitution did not uncouple NADPH oxidation from NO synthesis, because the NADPH oxidized per NO formed ratios remained similar (1.9 and 1.1 for mesohaem-nNOS compared with 2.1 and 1.1 for wild-type nNOS with L-Arg and NOHA as substrates respectively).

Haem midpoint potential

The Fe(III)/Fe(II) midpoint potential of wild-type and mesohaem-nNOSoxy proteins was determined at 15 °C for the L-Arg and

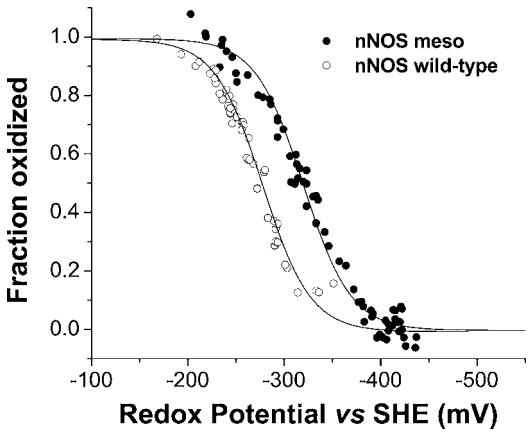

Figure 3 Redox titration of the wild-type and mesohaem-nNOSoxy proteins

Midpoint potentials for wild-type nNOSoxy and mesohaem-nNOSoxy were determined by fitting the fraction oxidized to the Nernst equation. The calculated E_m values were − 272 ± 2 mV for nNOSoxy wild-type and − 320 ± 2 mV for the mesohaem-nNOSoxy. See the Experimental section for details.

Table 3 Comparison of the thermodynamic and kinetic parameters of wild-type nNOS and mesohaem-nNOS

All measurements utilized nNOSoxy proteins and were made at 10 °C except for the midpoint potential (15 °C). Values shown are the means ± S.E.M.

Parameter	Wild-type nNOS	Mesohaem−nNOS
E_m Fe(III)/Fe(II) (mV)	− 272 ± 2	− 320 ± 2
Flavin reduction (s^{-1})	36.1 ± 0.6	40.2 ± 5.8
k_r (s^{-1})	6.6 ± 0.2	1.09 ± 0.01
k_{cat1} (s^{-1})	17.5 ± 0.2	52.1 ± 0.7
k_{cat2} (s^{-1})	23.8 ± 0.4	117 ± 6
k_{off} (s^{-1})	5.1 ± 0.1	8.2 ± 0.1
k_{ox} (s^{-1})	0.08 ± 0.005	0.19 ± 0.002

BH_4-bound enzymes (Figure 3). The calculated E_m values are shown in Table 3. The wild-type value agrees with other reports for nNOS [32,44,45], although those values were determined at 25 °C. The 48 mV decrease in midpoint potential we obtained for mesohaem-nNOS was similar to the 35−50 mV shifts reported for other mesohaem-substituted proteins, including cytochrome P450 and globins [14,17−19]. For mesohaem-nNOS, the downward 50 mV shift in midpoint potential places its haem Fe(III)/Fe(II) couple approx. 40 mV below the measured midpoint potential of the FMN HQ/SQ couple (approx. − 275 mV) [31,46]. This should create unfavourable thermodynamics for the electron transfer from the FMN-HQ to the Fe(III) mesohaem. Because this electron transfer is required for haem−O_2 binding and subsequent NO synthesis, the diminished thermodynamic driving force is expected to have an impact on nNOS catalysis.

Electron flux through the nNOS haem to O_2

In the presence of L-agmatine, a non-metabolizable L-Arg analogue, the rate of NADPH oxidation directly reflects the steady-state electron flux through the haem iron to O_2 [25,34]. Under these conditions, the wild-type nNOS had a 4-fold higher rate of NADPH oxidation than the mesohaem-nNOS, meaning the mesohaem substitution slows electron flux through the nNOS haem. Our measures of NADPH oxidation in the absence of substrate yielded comparable results (Table 2). These steady-state

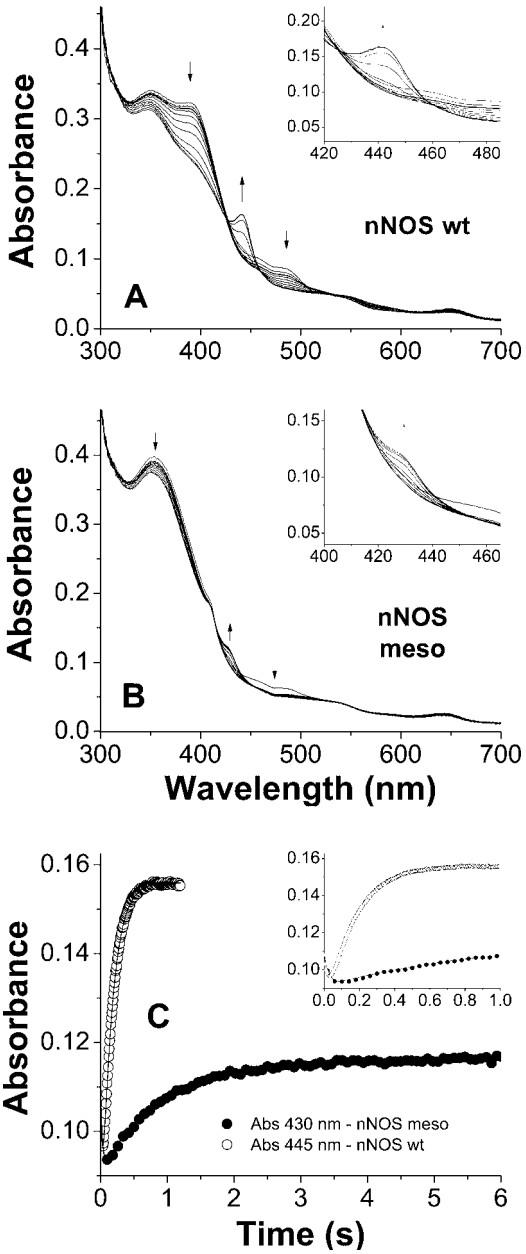

Figure 4 Kinetics of Fe(III) enzyme reduction in wild-type and mesohaem-nNOS proteins

Ferric enzyme (10 μM) was mixed with NADPH (100 μM) in CO-saturated buffer in the stopped-flow apparatus at 10 °C and build-up of the Fe(II)−CO peak (445 nm for wild-type, 430 nm for mesohaem-nNOS) was used to measure the rate of haem reduction. (**A**) Reaction of wild-type (wt) nNOS. The inset shows the Fe(II)−CO peak region. (**B**) Reaction of mesohaem-nNOS. The inset shows the Fe(II)−CO peak region. (**C**) Kinetic traces at the Fe(II)−CO peak wavelength for both proteins. The inset shows a shorter timescale.

measurments are consistent with a poor thermodynamic driving force for haem reduction in mesohaem-nNOS as predicted from its having a 50 mV lower haem midpoint potential.

Rate and extent of Fe(III) haem reduction

We directly assessed electron transfer from FMN to haem by measuring the rate and extent of haem reduction in mesohaem-nNOS using stopped-flow spectroscopy. The CaM-bound mesohaem and wild-type nNOS proteins were each mixed

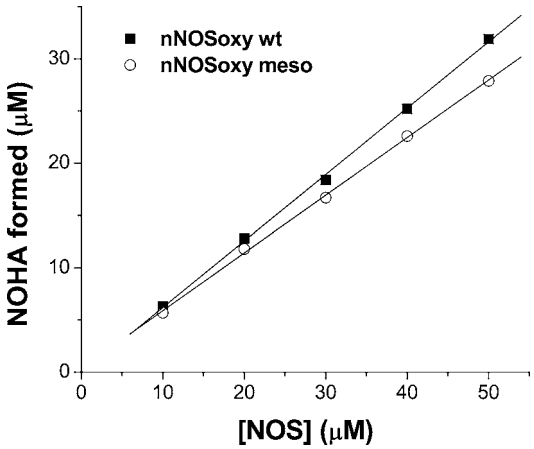

Figure 5 Yields of NOHA formation in the L-Arg single-turnover reactions

Ferrous L-Arg-bound nNOSoxy enzymes at the indicated concentrations were mixed with O_2-containing buffer to start the hydroxylation reaction, and the NOHA product was measured by HPLC. Results are the average from two replica experiments. S.D. of the data points $\leqslant$0.4 μM. wt, wild-type.

with NADPH in a stopped-flow spectrophotometer at 10 °C under an N_2/CO atmosphere and the resulting haem reduction was monitored by formation of the Fe(II)−CO complex at 430 nm or 445 nm respectively. Representative diode array spectra and kinetic traces at the diagnostic wavelengths are shown in Figure 4. There was a lesser extent of haem reduction achieved in the mesohaem-nNOS as indicated by its reaching only approx. 30 % the level of Fe(II)−CO complex formation relative to the wild-type (Figure 4). These different extents of haem reduction were also apparent in the kinetic traces constructed from the data at 444 nm and 430 nm (Figure 4C). We fit the kinetic traces to a bi-exponential function, with the initial fast phase representing an absorbance decrease at these wavelengths due to flavin reduction, and the subsequent slow phase representing the rate of haem reduction in the presence of CO. The fitted values (flavin reduction and k_r) are shown in Table 3. The values indicate that mesohaem-nNOS has normal flavin reduction kinetics, but a 6-fold lower rate of haem reduction. The lower rate and extent of haem reduction in the mesohaem-nNOS is similar to what we found previously in the W409F and W409Y mutants of nNOS [23], which contain native protohaem but have more negative haem midpoint potentials (J. Tejero, D. Stuehr, S. Daff and T. Ost, unpublished work), owing to an effect of these mutations on the electronics of the haem−thiolate bond. Taken together, the current results suggest that the slower haem reduction in mesohaem-nNOS is primarily due to the poor thermodynamic driving force brought on by the change in the Fe(III)/Fe(II) midpoint potential, and is probably not due to the modest structural change in the mesoporphyrin (i.e. replacement of the 2- and 4-vinyl groups with ethyl groups).

Single-turnover reactions of L-Arg and NOHA oxidation

To understand how the mesohaem substitution may have an impact on nNOS catalytic parameters other than k_r (i.e. k_{cat}, k_{ox} and k_{off} depicted in Figure 1B), we investigated L-Arg hydroxylation and NOHA oxidation in single-turnover reactions catalysed by nNOSoxy proteins at 10 °C. We first quantified NOHA formation from L-Arg during the single-turnover reaction (Figure 5). We found similar product yields for wild-type and mesohaem-containing nNOSoxy proteins (0.63 ± 0.01 and 0.56 ± 0.01 NOHA per haem respectively). Their similar efficiencies for L-Arg hydroxylation is consistent with the mesohaem substitution

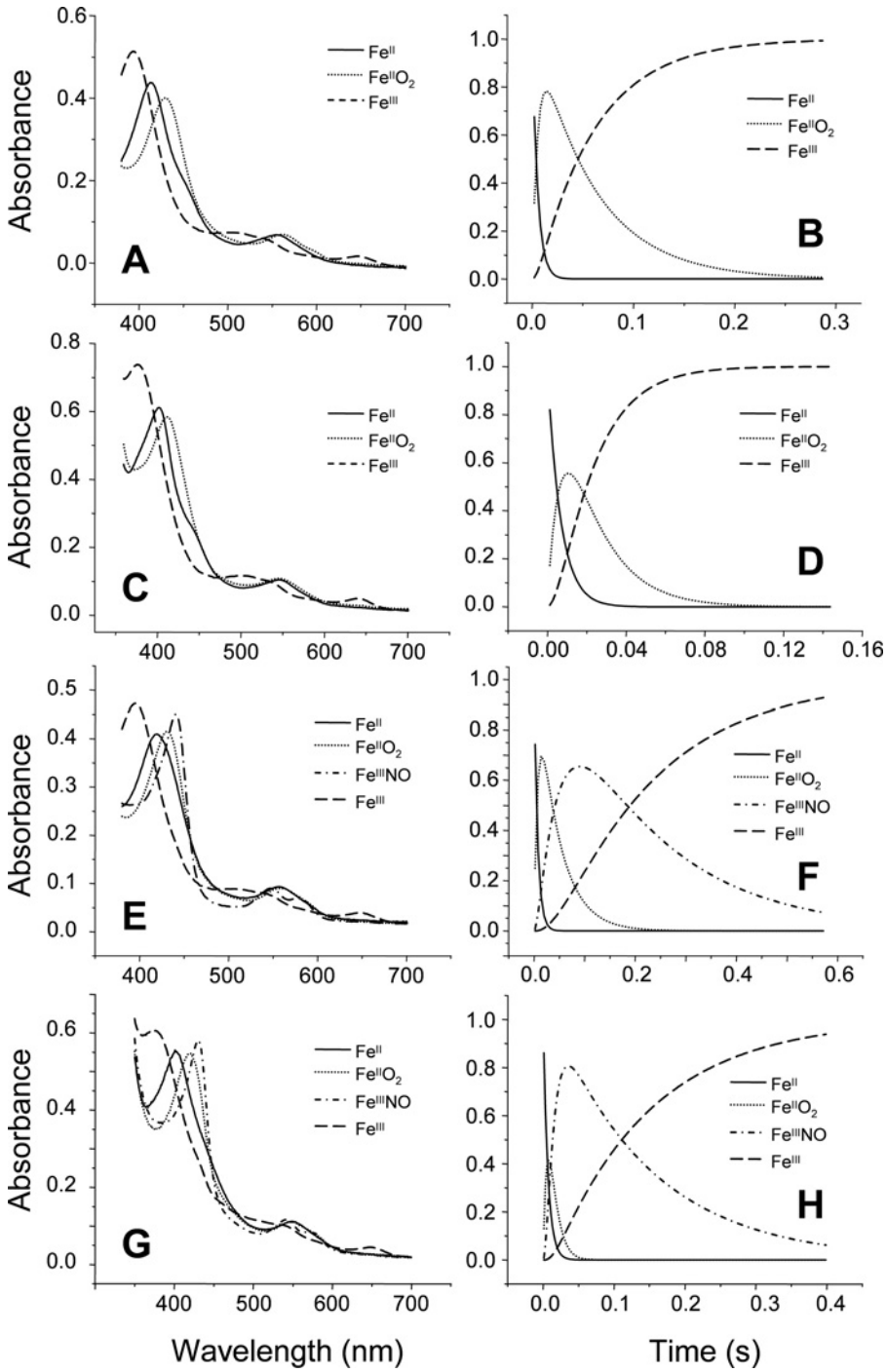

Figure 6 Stopped-flow analysis of haem transitions during single-turnover reactions

Ferrous nNOSoxy was mixed with air-saturated buffer in the stopped-flow apparatus at 10 °C in the presence of BH_4 and either L-Arg or NOHA. The left-hand panels show the species detected by global analysis of the spectral data in each reaction; right-hand panels show the concentration profiles of each species against time for the corresponding reaction in the left-hand panels. (**A** and **B**) Reaction of wild-type nNOSoxy with L-Arg. (**C** and **D**) Reaction of mesohaem-nNOSoxy with L-Arg. (**E** and **F**) Reaction of wild-type nNOSoxy with NOHA. (**G** and **H**) Reaction of mesohaem-nNOSoxy with NOHA.

being tolerated by the protein and its not increasing uncoupled O_2 reduction during steady-state NO synthesis by nNOS (Table 2).

We then used stopped-flow spectroscopy [35,36] to document and compare the nNOSoxy haem and mesohaem transitions that occur during the single-turnover reactions. The reactions were initiated by rapid-mixing an oxygen-containing buffer with pre-reduced Fe(II) nNOSoxy proteins that contained BH_4 and either L-Arg or NOHA as substrate. For the L-Arg reactions we observed two consecutive haem transitions: Fe(II)→Fe(II)−O_2→Fe(III) and in the reaction with NOHA we observed three transitions: Fe(II)→Fe(II)−O_2→Fe(III)−NO→Fe(III). Global analysis of the spectral data according to these models yielded the spectrum of each species (Figure 6, left-hand panels). All mesohaem-nNOSoxy species displayed Soret absorbance peaks that were

Table 4 Calculated rates for the haem transitions observed during L-Arg or NOHA single-turnover reactions performed at 10 °C

Values shown are measn ± S.E.M. (a) Represents the transition Fe(II)→Fe(II)−O_2→Fe(III). (b) Represents the transition Fe(II)→Fe(II)−O_2→Fe(III)−NO→Fe(III)

(a)

		Observed transition rates (s^{-1})	
Single-turnover reaction	Enzyme	Fe(II)→Fe(II)−O_2	Fe(II)−O_2→Fe(III)
BH_4, L-Arg	Wild-type nNOSoxy	183 ± 11	17.5 ± 0.2
	Mesohaem−nNOSoxy	168 ± 7	52.1 ± 0.7

(b)

		Observed transition rates (s^{-1})		
Single-turnover reaction	Enzyme	Fe(II)→Fe(II)−O_2	Fe(II)−O_2→Fe(III)−NO	Fe(III)−NO→Fe(III)
BH_4, NOHA	Wild-type nNOSoxy	133 ± 6	23.8 ± 0.4	5.1 ± 0.1
	Mesohaem−nNOSoxy	153 ± 13	117 ± 6	8.2 ± 0.1

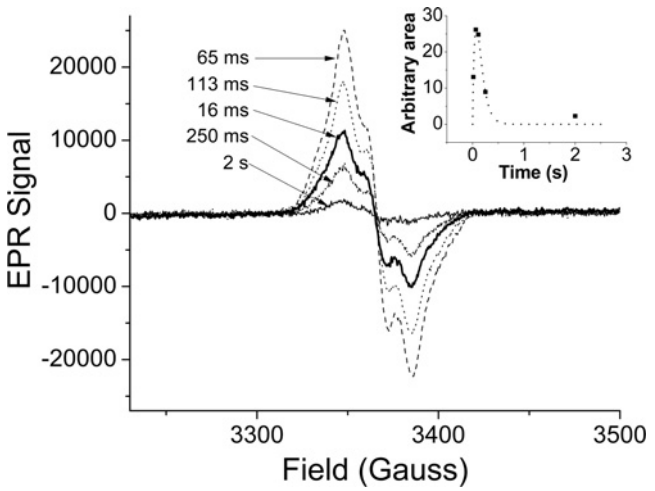

Figure 7 BH_4 radical formation during the L-Arg single-turnover reaction catalysed by mesohaem-nNOSoxy

Ferrous enzyme was rapid-mixed with O_2-containing buffer and the reactions were freeze-quenched at the times indicated. The EPR spectra of reaction samples frozen at each time point are shown. Inset: kinetics of BH_4 radical signal build-up and decay. Points indicate the calculated concentration of radical in arbitrary units. The dotted line indicates a tentative fit to the data.

shifted ∼15 nm towards a shorter wavelength as compared with wild-type nNOSoxy. This is an expected consequence of the mesohaem substitution [11−16]. The transition rates are reported in Table 4. In general, the transition rates for the mesohaem-nNOSoxy reactions were higher than those for wild-type (Table 4), with the main difference being the step that represents the reduction and subsequent reactivity of the common Fe(II)−O_2 complex that forms in both the L-Arg and NOHA single-turnover reactions (k_{cat1} and k_{cat2} in Figure 1). This step was 3-fold higher in the L-Arg reaction and 5-fold higher in the NOHA reactions catalysed by mesohaem-nNOSoxy (Tables 3 and 4). Enhanced rates of oxygen activation and reactivity with substrates has also been observed in other haem−thiolate enzymes when their haem midpoint potentials become more negative [47,48]. Based on our previous work [23−25], our kinetic data with mesohaem-nNOSoxy implies that its Fe(II)−O_2 complex is likely to become reduced by BH_4 more quickly than in wild-type nNOSoxy during both steps of NO synthesis. Using single-turnover rapid-freeze experiments, we confirmed that the BH_4 radical does form in mesohaem-nNOSoxy during the L-Arg hydroxylation reaction (Figure 7). In general, the BH_4 radical formation was similar to that previously observed in the wild-type nNOSoxy reaction [35,40,49], except that the BH_4 radical appeared to decay faster in the mesohaem-nNOSoxy reaction. However, this apparent change in BH_4 radical stability did not diminish the efficiency of mesohaem-nNOS with regard to its NADPH oxidation and NO synthesis (Table 2).

In the NOHA single-turnover reactions, we observed build-up of an immediate Fe(III)−NO product complex that is typically seen in the wild-type nNOSoxy reaction [36,37] (Figure 6), and so could determine the macroscopic off-rate of NO from this product complex by monitoring its transition to Fe(III) enzyme (k_{off} parameter in Figure 1B). The analysis showed that mesohaem-nNOSoxy had a higher NO k_{off} compared with wild-type (Tables 3 and 4).

In summary, we found that all observable haem transitions that represent the various catalytic events occurring downstream from formation of the Fe(II)−O_2 species were faster in mesohaem-nNOSoxy in both the L-Arg and NOHA single-turnover reactions. This indicates that the mesohaem substitution gives nNOS some improved catalytic properties.

Ferrous haem−NO oxidation (k_{ox})

During NO synthesis, a portion of the Fe(III) haem−NO product complex is reduced by the attached reductase domain and the resulting Fe(II) haem−NO complex must then react with O_2 (k_{ox} in Figure 1B) to return to the catalytic cycle [6]. We used stopped-flow spectroscopy to determine whether the mesohaem substitution alters the k_{ox} parameter in nNOSoxy. The time course results for the mesohaem-nNOSoxy reaction is shown in Figure 8. As in wild-type nNOSoxy [21], the Fe(II) mesohaem−NO complex converted into Fe(III) enzyme with clear spectral isosbestic points and no apparent formation of intermediate species. The transition rates obtained at either 424 nm [Fe(II)−NO decay] or 378 nm [Fe(III) build-up] were similar and yielded an average k_{ox} rate more than twice as high as the k_{ox} value measured for wild-type nNOSoxy under identical conditions (Table 3). The higher k_{ox} of mesohaem-nNOS is consistent with previous results we obtained with W409F and W409Y mutants of nNOS, which also have lower haem midpoint potentials and higher k_{ox} values relative to wild-type [24,25]. A higher k_{ox}, on its own, can increase the steady-state activity of nNOS by speeding the return of enzyme molecules to the productive cycle (Figure 1B) [6,21,22].

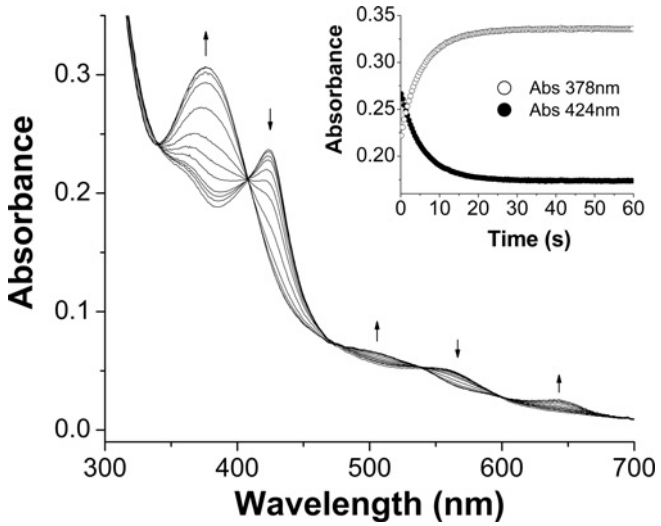

Figure 8 Kinetics of O_2 reaction with the mesohaem-nNOSoxy Fe(II)−NO complex

Ferrous−NO complex (10 μM) was mixed with air-saturated buffer (O_2 concentration $\approx$ 280 μM) in the stopped-flow apparatus at 10 °C and sequential spectra were recorded. Inset: kinetics of absorbance changes at 378 nm [Fe(III) build-up] and 424 nm [Fe(II)−NO decay] and fittings to single exponential equations.

Modelling catalysis by the mesohaem-containing nNOS

The model depicted in Figure 1(B) illustrates how several catalytic parameters (k_r, k_{cat}, k_{off} and k_{ox}) influence the steady-state NO synthesis activity of NOS enzymes [6,21,22]. We used the kinetic values obtained for mesohaem-nNOS in a computer simulation of a kinetic model similar to that depicted in Figure 1(B) to determine whether the alterations we observed in the kinetic parameters could explain the steady-state catalytic behaviours of mesohaem-nNOS. The predicted distributions for wild-type and mesohaem-nNOS are compared in Figure 9. The kinetic parameters of the wild-type enzyme are such that it primarily populates the Fe(II)−NO form, as described previously [22,25,38]. In contrast, the altered kinetic parameters of mesohaem-nNOS predict that it should primarily populate the Fe(III) form and have a much-diminished population of the Fe(II) haem−NO species. To test these predictions we recorded UV−visible spectra of the wild-type and mesohaem-nNOS during their steady-state NO synthesis reactions (Figure 9, middle and lower panels). The difference in mesohaem-nNOS enzyme distribution predicted by the simulation [diminished Fe(II)−NO and increased Fe(III) species] was observed during steady-state NO synthesis. In wild-type nNOS, the haem−NO species built-up within 2 s after starting the reaction, and its build-up coincided with a marked deflection in enzyme NADPH consumption, which occurs as a consequence of, and in proportion to, the build-up of this species [42]. A significant shift to the haem−NO species during steady-state catalysis is also apparent from the difference spectrum (steady-state minus initial) determined for the wild-type nNOS reaction (Figure 9 inset), which shows a clear loss of Fe(III) enzyme absorbance at 395 nm and gain in Fe(II)−NO species absorbance. In contrast, all of the changes that are characteristic of a redistribution to the Fe(II)−NO species are muted in the mesohaem-nNOS data set, which shows very little deflection in NADPH oxidation, loss of Fe(III) enzyme or gain in Fe(II)−NO species.

The altered distribution of mesohaem-nNOS can be attributed to the lower k_r and higher k_{off}. Together, these rates determine the partition ratio (k_{off}/k_r) of the Fe(III) haem−NO product complex (see Figure 1B). In wild-type nNOS the k_{off} and k_r values are set such that they give a partition ratio of nearly 1:1, whereas in mesohaem-nNOS the parameters have been reset to give a partition ratio of 8:1. This change keeps the majority of mesohaem-nNOS in the productive cycle of NO synthesis and release, and diminishes the amount of molecules that circulate in the futile NO dioxygenase cycle, thus diminishing build-up of the Fe(II)−NO species. The higher k_{ox} of mesohaem-nNOS can also help to alter the enzyme distribution and diminish Fe(II)−NO build-up, but contributes to a lesser extent than does the change in the partition ratio. Interestingly, the distribution for mesohaem-nNOS shown in the present paper is similar to the distribution for the W409F nNOS, mutant during its steady-state NO synthesis [6,23]. However, in W409F nNOS, the altered distribution is mostly due to a large increase in k_{ox} (7-fold higher than in wild-type nNOS), and is due less to an altered partition ratio (the k_{off}/k_r is 2.8 for this mutant). This shows how different changes in the enzyme kinetic parameters can lead to similar changes in NOS enzyme distribution during NO synthesis.

NO synthesis activity compared with O_2 concentration (K_mO_2)

We measured the NO synthesis activities of the wild-type and mesohaem-nNOS at different oxygen concentrations. Figure 10 (left-hand panel) compares plots of the measured activities against O_2 concentration data for both enzyme forms. The mesohaem-nNOS had a lower V_{max} and also had a decreased apparent K_mO_2 value. For comparison, the simulated activity against O_2 concentration curves derived for the wild-type and mesohaem-nNOS using our measured kinetic parameters are shown in Figure 10 (right-hand panels). In general, the simulated curves match the trends we observed for the experimental data, also giving mesohaem-nNOS a lower V_{max} and a lower K_mO_2 than wild-type (Figure 10). There is some divergence between the simulated and actual values and the magnitude of change, in particular for the change in the apparent K_mO_2 of mesohaem-nNOS. This may be due to measurement errors, and may also reflect our deriving the simulated curves from kinetic data at 10 °C. In any case, the lower V_{max} of mesohaem-nNOS is consistent with its lower haem reduction rate, because the kinetic model stipulates that the k_r will become rate-limiting for the NO synthesis activity at high O_2 concentrations (i.e. where k_{ox} becomes higher). The lower K_mO_2 of mesohaem-nNOS is also consistent with its lower k_r and higher k_{ox}, which together diminish the importance of the Fe(II)−NO reaction with O_2 in determining the apparent K_mO_2 of the enzyme. Similar changes in the k_r and k_{ox} parameters occur in nNOS Trp^{409} and Glu^{762} mutants, and also significantly lower their apparent K_mO_2 [6,23,24,41].

Summary and conclusions

In the present study we successfully employed a bacterial haem transporter system to overexpress mesohaem-containing nNOS. The midpoint potential of the bound mesohaem was 50 mV lower than the native haem cofactor. The mesohaem substitution caused changes in the enzyme k_r, k_{cat}, k_{ox} and NO k_{off} values, which, in most cases, could be attributed to the altered electronics of the bound mesohaem. Despite its altered kinetic parameters, mesohaem-nNOS was catalytically efficient as an NO synthase and even performed certain catalytic transitions faster than does the wild-type enzyme, in particular the transitions associated with oxygen activation and reaction with substrate. Mesohaem nNOS had lower V_{max} and K_mO_2 values for its NO synthesis activity compared with wild-type enzyme. Thus a more

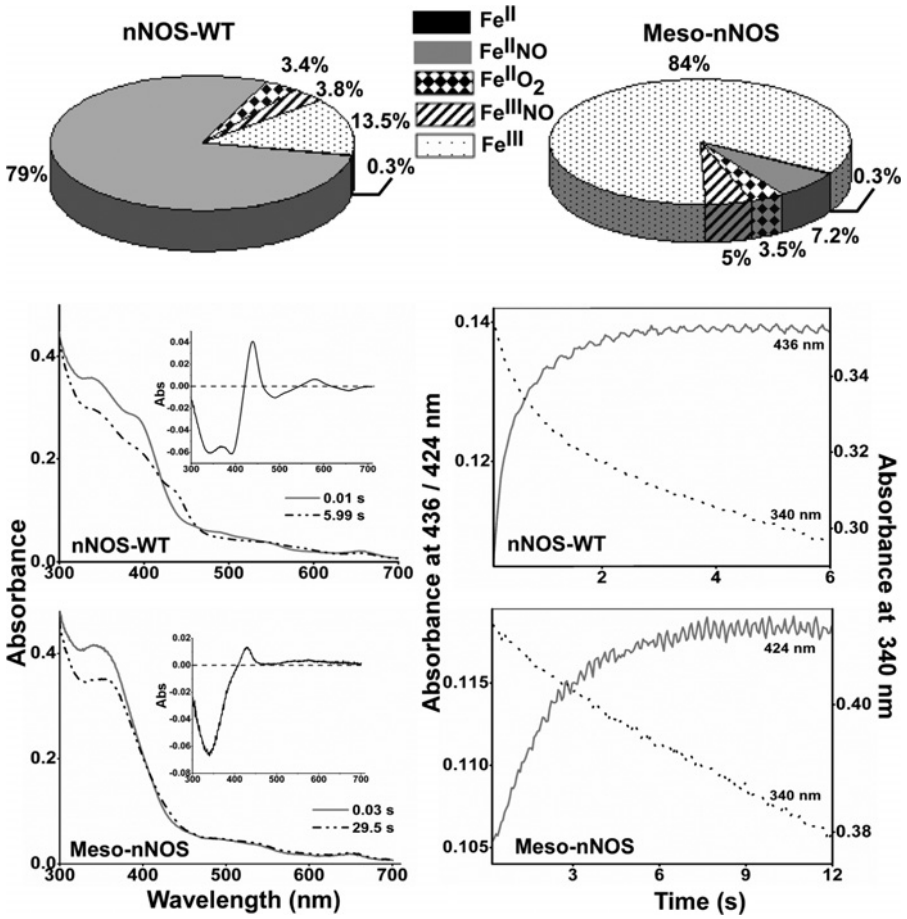

Figure 9 Simulated and observed distribution of wild-type (WT) and mesohaem-nNOS during their steady-state NO synthesis

Upper panel: the distributions were calculated by utilizing measured kinetic parameters in simulations of a global kinetic model (see Figure 1), assuming constant concentrations of O_2 (180 μM, i.e. one-half of air-saturated oxygen concentration at 10 °C) and NADPH (40 μM) and no build-up of NO in solution. Middle and lower panels: left-hand panels, spectra of the pre-steady-state (continuous line) and steady-state (broken line) enzymes were recorded at the times indicated after initiating NO synthesis from L-Arg in a stopped-flow spectrophotometer. Insets show the steady-state minus pre-steady state difference spectra. Middle and lower panels: right-hand panels, kinetics of absorbance change at the wavelengths indicated recorded during the NO synthesis reaction.

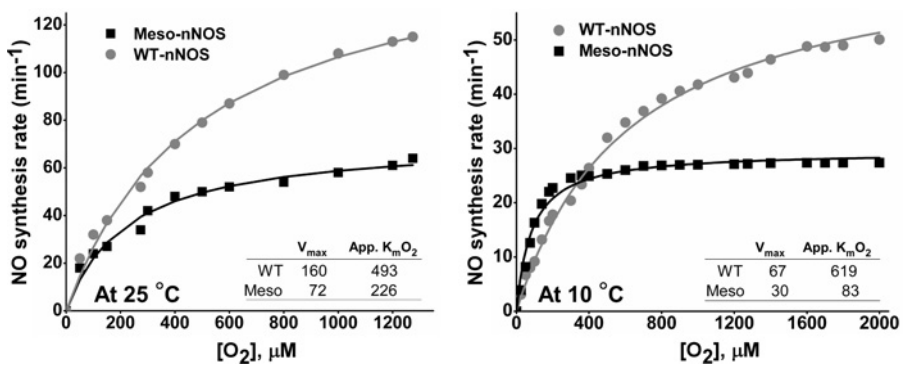

Figure 10 Measured and simulated oxygen-dependence of the NO synthesis activities

Left-hand panel: rates of NO synthesis at 25 °C were measured at the O_2 concentrations indicated for wild-type and mesohaem-nNOS proteins. Right-hand panel: simulations of a kinetic model were run using kinetic values obtained at 10 °C for each O_2 concentration indicated to derive the simulated NO synthesis activities at 10 °C. In both panels, points were fitted to the Michaelis–Menten equation to give the indicated lines of fit. Reported values are in min^{-1} (V_{max}) and μM (K_mO_2). WT, wild-type.

negative redox potential appears to be beneficial for the NO synthesis reactions occurring in the haem domain, but becomes counterproductive as soon as the electron transfer from the FMN becomes compromised. It is reasonable to think that the redox potential of the NOS haem has evolved to be as low as possible while being close to the FMN HQ/SQ midpoint potential. The altered catalytic behaviours observed in mesohaem-nNOS were attributable to the observed changes in the kinetic parameters, as indicated when we incorporated the kinetic values measured for mesohaem-nNOS into computer simulations of a global kinetic model for NOS. Taken together, our results present a comprehensive and detailed demonstration of how changes in

haem electronics can affect multiple kinetic parameters in nNOS, and how these changes combine to alter its catalytic behaviours.

AUTHOR CONTRIBUTION

Jesús Tejero, Ashis Biswas, Mohammad Mahfuzul Haque and Zhi-Qiang Wang performed experiments and analysed data. Craig Hemann performed the EPR experiments. Russ Hille provided the EPR equipment. Cornelius Varnado and Douglas Goodwin contributed the haem transporter protein and technical advice. Zachary Novince developed the expression protocol for the mesohaem-containing proteins. Jesùs Tejero, Ashis Biswas and Mohammad Mahfuzul drafted the manuscript. Dennis Stuehr designed the research, analysed data and wrote the final manuscript.

FUNDING

This work was supported by the National Institutes of Health [grant numbers CA53914, GM51491 (to D.J.S.), GM 075036 (to R.H.)] and American Heart Association postdoctoral fellowships [grant numbers 0825545D (to A.B.), 0625632B (to J.T.)].

REFERENCES

1 Pfeiffer, S., Mayer, B. and Hemmens, B. (1999) Nitric oxide: chemical puzzles posed by a biological messenger. Angew. Chem. Int. Ed. **38**, 1714–1731
2 Garcin, E. D., Bruns, C. M., Lloyd, S. J., Hosfield, D. J., Tiso, M., Gachhui, R., Stuehr, D. J., Tainer, J. A. and Getzoff, E. D. (2004) Structural basis for isozyme-specific regulation of electron transfer in nitric-oxide synthase. J. Biol. Chem. **279**, 37918–37927
3 Xia, C., Misra, I., Iyanagi, T. and Kim, J. J. (2009) Regulation of interdomain interactions by calmodulin in inducible nitric-oxide synthase. J. Biol. Chem. **284**, 30708–30717
4 Crane, B. R., Arvai, A. S., Ghosh, D. K., Wu, C., Getzoff, E. D., Stuehr, D. J. and Tainer, J. A. (1998) Structure of nitric oxide synthase oxygenase dimer with pterin and substrate. Science **279**, 2121–2126
5 Abu-Soud, H. M., Yoho, L. L. and Stuehr, D. J. (1994) Calmodulin controls neuronal nitric-oxide synthase by a dual mechanism. Activation of intra- and interdomain electron transfer. J. Biol. Chem. **269**, 32047–32050
6 Stuehr, D. J., Santolini, J., Wang, Z. Q., Wei, C. C. and Adak, S. (2004) Update on mechanism and catalytic regulation in the NO synthases. J. Biol. Chem. **279**, 36167–36170
7 Gorren, A. C. F. and Mayer, B. (2007) Nitric-oxide synthase: a cytochrome P450 family foster child. Biochim. Biophys. Acta **1770**, 432–445
8 Wei, C. C., Crane, B. R. and Stuehr, D. J. (2003) Tetrahydrobiopterin radical enzymology. Chem. Rev. **103**, 2365–2383
9 Bender, A. T., Kamada, Y., Kleaveland, P. A. and Osawa, Y. (2002) Assembly and activation of heme-deficient neuronal NO synthase with various porphyrins. J. Inorg. Biochem. **91**, 625–634
10 Woodward, J. J., Martin, N. I. and Marletta, M. A. (2007) An *Escherichia coli* expression-based method for heme substitution. Nat. Methods **4**, 43–45
11 Tamura, M., Asakura, T. and Yonetani, T. (1973) Heme modification studies of myoglobin. I. Purification and some optical and EPR characteristics of synthesized myoglobins containing unnatural hemes. Biochim. Biophys. Acta **295**, 467–479
12 Modi, S., Primrose, W. U., Lian, L. Y. and Roberts, G. C. (1995) Effect of replacement of ferriprotoporphyrin IX in the haem domain of cytochrome P-450 BM-3 on substrate binding and catalytic activity. Biochem. J. **310**, 939–943
13 Antonini, E., Brunori, M., Caputo, A., Chiancone, E., Fanelli, A. R. and Wyman, J. (1964) Studies on the structure of hemoglobin. III. Physicochemical properties of reconstituted hemoglobins. Biochim. Biophys. Acta **79**, 284–292
14 Ryabova, E. S., Rydberg, P., Kolberg, M., Harbitz, E., Barra, A. L., Ryde, U., Andersson, K. K. and Nordlander, E. (2005) A comparative reactivity study of microperoxidases based on hemin, mesohemin and deuterohemin. J. Inorg. Biochem. **99**, 852–863
15 Makino, R. and Yamazaki, I. (1972) Effects of 2,4-substituents of deuterohemin upon peroxidase functions. I. Preparation and some properties of artificial enzymes. J. Biochem. (Tokyo) **72**, 655–664
16 Singh, U. P., Obayashi, E., Takahashi, S., Iizuka, T., Shoun, H. and Shiro, Y. (1998) The effects of heme modification on reactivity, ligand binding properties and iron-coordination structures of cytochrome P450nor. Biochim. Biophys. Acta **1384**, 103–111
17 Brunori, M., Saggese, U., Rotilio, G. C., Antonini, E. and Wyman, J. (1971) Redox equilibrium of sperm-whale myoglobin, *Aplysia* myoglobin, and *Chironomus thummi* hemoglobin. Biochemistry **10**, 1604–1609
18 Yamada, H., Makino, R. and Yamazaki, I. (1975) Effects of 2,4-substituents of deuteropheme upon redox potentials of horseradish peroxidases. Arch. Biochem. Biophys. **169**, 344–353
19 Flaherty, M. M., Rish, K. R., Smith, A. and Crumbliss, A. L. (2008) An investigation of hemopexin redox properties by spectroelectrochemistry: biological relevance for heme uptake. Biometals **21**, 239–248
20 Ignarro, L. J., Ballot, B. and Wood, K. S. (1984) Regulation of soluble guanylate cyclase activity by porphyrins and metalloporphyrins. J. Biol. Chem. **259**, 6201–6207
21 Santolini, J., Meade, A. L. and Stuehr, D. J. (2001) Differences in three kinetic parameters underpin the unique catalytic profiles of nitric-oxide synthases I, II, and III. J. Biol. Chem. **276**, 48887–48898
22 Santolini, J., Adak, S., Curran, C. M. and Stuehr, D. J. (2001) A kinetic simulation model that describes catalysis and regulation in nitric-oxide synthase. J. Biol. Chem. **276**, 1233–1243
23 Adak, S. and Stuehr, D. J. (2001) A proximal tryptophan in NO synthase controls activity by a novel mechanism. J. Inorg. Biochem. **83**, 301–308
24 Adak, S., Wang, Q. and Stuehr, D. J. (2000) Molecular basis for hyperactivity in tryptophan 409 mutants of neuronal NO synthase. J. Biol. Chem. **275**, 17434–17439
25 Adak, S., Crooks, C., Wang, Q., Crane, B. R., Tainer, J. A., Getzoff, E. D. and Stuehr, D. J. (1999) Tryptophan 409 controls the activity of neuronal nitric-oxide synthase by regulating nitric oxide feedback inhibition. J. Biol. Chem. **274**, 26907–26911
26 Tejero, J., Biswas, A., Wang, Z. Q., Page, R. C., Haque, M. M., Hemann, C., Zweier, J. L., Misra, S. and Stuehr, D. J. (2008) Stabilization and characterization of a heme-oxy reaction intermediate in inducible nitric-oxide synthase. J. Biol. Chem. **283**, 33498–33507
27 Lang, J., Driscoll, D., Gelinas, S., Rafferty, S. P. and Couture, M. (2009) Trp^{180} of endothelial NOS and Trp^{56} of bacterial saNOS modulate σ bonding of the axial cysteine to the heme. J. Inorg. Biochem. **103**, 1102–1112
28 Varnado, C. L. and Goodwin, D. C. (2004) System for the expression of recombinant hemoproteins in *Escherichia coli*. Protein Expression Purif. **35**, 76–83
29 Abu-Soud, H. M., Gachhui, R., Raushel, F. M. and Stuehr, D. J. (1997) The ferrous-dioxy complex of neuronal nitric oxide synthase. Divergent effects of L-arginine and tetrahydrobiopterin on its stability. J. Biol. Chem. **272**, 17349–17353
30 Adak, S., Ghosh, S., Abu-Soud, H. M. and Stuehr, D. J. (1999) Role of reductase domain cluster 1 acidic residues in neuronal nitric-oxide synthase. Characterization of the FMN-free enzyme. J. Biol. Chem. **274**, 22313–22320
31 Ilagan, R. P., Tiso, M., Konas, D. W., Hemann, C., Durra, D., Hille, R. and Stuehr, D. J. (2008) Differences in a conformational equilibrium distinguish catalysis by the endothelial and neuronal nitric-oxide synthase flavoproteins. J. Biol. Chem. **283**, 19603–19615
32 Presta, A., Weber-Main, A. M., Stankovich, M. T. and Stuehr, D. (1998) Comparative effects of substrates and pterin cofactor on the heme midpoint potential in inducible and neuronal nitric oxide synthases. J. Am. Chem. Soc. **120**, 9460–9465
33 Panda, K., Haque, M. M., Garcin-Hosfield, E. D., Durra, D., Getzoff, E. D. and Stuehr, D. J. (2006) Surface charge interactions of the FMN module govern catalysis by nitric-oxide synthase. J. Biol. Chem. **281**, 36819–36827
34 Haque, M. M., Panda, K., Tejero, J., Aulak, K. S., Fadlalla, M. A., Mustovich, A. T. and Stuehr, D. J. (2007) A connecting hinge represses the activity of endothelial nitric oxide synthase. Proc. Natl. Acad. Sci. U.S.A. **104**, 9254–9259
35 Wei, C. C., Wang, Z. Q., Wang, Q., Meade, A. L., Hemann, C., Hille, R. and Stuehr, D. J. (2001) Rapid kinetic studies link tetrahydrobiopterin radical formation to heme-dioxy reduction and arginine hydroxylation in inducible nitric-oxide synthase. J. Biol. Chem. **276**, 315–319
36 Wei, C. C., Wang, Z. Q. and Stuehr, D. J. (2002) Nitric oxide synthase: use of stopped-flow spectroscopy and rapid-quench methods in single-turnover conditions to examine formation and reactions of heme-O_2 intermediate in early catalysis. Methods Enzymol. **354**, 320–338
37 Boggs, S., Huang, L. and Stuehr, D. J. (2000) Formation and reactions of the heme-dioxygen intermediate in the first and second steps of nitric oxide synthesis as studied by stopped-flow spectroscopy under single-turnover conditions. Biochemistry **39**, 2332–2339
38 Abu-Soud, H. M., Rousseau, D. L. and Stuehr, D. J. (1996) Nitric oxide binding to the heme of neuronal nitric-oxide synthase links its activity to changes in oxygen tension. J. Biol. Chem. **271**, 32515–32518
39 Salerno, J. C. and Ghosh, D. K. (2009) Space, time and nitric oxide: neuronal nitric oxide synthase generates signal pulses. FEBS J. **276**, 6677–6688
40 Wei, C. C., Wang, Z. Q., Tejero, J., Yang, Y. P., Hemann, C., Hille, R. and Stuehr, D. J. (2008) Catalytic reduction of a tetrahydrobiopterin radical within nitric-oxide synthase. J. Biol. Chem. **283**, 11734–11742
41 Haque, M. M., Fadlalla, M., Wang, Z. Q., Ray, S. S., Panda, K. and Stuehr, D. J. (2009) Neutralizing a surface charge on the FMN subdomain increases the activity of neuronal nitric-oxide synthase by enhancing the oxygen reactivity of the enzyme heme-nitric oxide complex. J. Biol. Chem. **284**, 19237–19247

42 Abu-Soud, H. M., Wang, J., Rousseau, D. L., Fukuto, J. M., Ignarro, L. J. and Stuehr, D. J. (1995) Neuronal nitric oxide synthase self-inactivates by forming a ferrous-nitrosyl complex during aerobic catalysis. J. Biol. Chem. **270**, 22997–23006
43 Ghosh, D. K., Crane, B. R., Ghosh, S., Wolan, D., Gachhui, R., Crooks, C., Presta, A., Tainer, J. A., Getzoff, E. D. and Stuehr, D. J. (1999) Inducible nitric oxide synthase: role of the N-terminal β-hairpin hook and pterin-binding segment in dimerization and tetrahydrobiopterin interaction. EMBO J. **18**, 6260–6270
44 Gao, Y. T., Smith, S. M., Weinberg, J. B., Montgomery, H. J., Newman, E., Guillemette, J. G., Ghosh, D. K., Roman, L. J., Martasek, P. and Salerno, J. C. (2004) Thermodynamics of oxidation-reduction reactions in mammalian nitric-oxide synthase isoforms. J. Biol. Chem. **279**, 18759–18766
45 Ost, T. W. and Daff, S. (2005) Thermodynamic and kinetic analysis of the nitrosyl, carbonyl, and dioxy heme complexes of neuronal nitric-oxide synthase. The roles of substrate and tetrahydrobiopterin in oxygen activation. J. Biol. Chem. **280**, 965–973
46 Noble, M. A., Munro, A. W., Rivers, S. L., Robledo, L., Daff, S. N., Yellowlees, L. J., Shimizu, T., Sagami, I., Guillemette, J. G. and Chapman, S. K. (1999) Potentiometric analysis of the flavin cofactors of neuronal nitric oxide synthase. Biochemistry **38**, 16413–16418
47 Yoshioka, S., Takahashi, S., Ishimori, K. and Morishima, I. (2000) Roles of the axial push effect in cytochrome P450cam studied with the site-directed mutagenesis at the heme proximal site. J. Inorg. Biochem. **81**, 141–151
48 Matsumura, H., Wakatabi, M., Omi, S., Ohtaki, A., Nakamura, N., Yohda, M. and Ohno, H. (2008) Modulation of redox potential and alteration in reactivity via the peroxide shunt pathway by mutation of cytochrome P450 around the proximal heme ligand. Biochemistry **47**, 4834–4842
49 Wei, C. C., Wang, Z. Q., Durra, D., Hemann, C., Hille, R., Garcin, E. D., Getzoff, E. D. and Stuehr, D. J. (2005) The three nitric-oxide synthases differ in their kinetics of tetrahydrobiopterin radical formation, heme-dioxy reduction, and arginine hydroxylation. J. Biol. Chem. **280**, 8929–8935

Received 23 August 2010/7 October 2010; accepted 15 October 2010
Published as BJ Immediate Publication 15 October 2010, doi:10.1042/BJ20101353